Engineering Structures 343 (2025) 121117

Contents lists available at ScienceDirect

Engineering Structures

journal homepage: www.elsevier.com/locate/engstruct

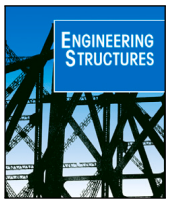

Static and fatigue performance of glass fiber-reinforced polymer (GFRP) web-core bridge deck sandwich panels: Experimental and numerical investigation

Olena Karpenko, Marko Pavlovic *

Delft University of Technology, Stevinweg 1, Delft, 2628CN, Netherlands

ARTICLE INFO

Keywords:
Web-core sandwich panels
Fatigue performance
Experimental investigation
European standards
Bridge decks
Imperfections

ABSTRACT

This study investigates the static and fatigue performance of glass fiber-reinforced polymer web-core bridge deck sandwich panels through experimental testing and numerical analysis. Tested deck specimens, incorporating reduced facing and web thicknesses to approximately 50% of full-scale decks, were designed to capture critical failure modes while maintaining realistic geometry and support conditions. The web-core sandwich panels, spanning 2 meters, demonstrated an ultimate load capacity exceeding 450 kN, which is more than 10 times higher than the factored highway wheel load defined by FLM4 (0.5*90 kN) and over 4 times higher the LM2 wheel load (0.5*200 kN), underscoring their potential for real-world bridge applications. The fatigue tests revealed multiple failure modes at high loads, with imperfections identified as the primary cause of failure. Finite Element Analysis supports the experimental results, showing that imperfections significantly reduce fatigue life, increasing local stresses and reducing the number of cycles. The buckling analysis suggested by the current European design recommendations was found to be conservative, as web buckling was not observed in tests. These findings underline the importance of accounting for imperfections in the design verifications, with further research needed to validate these conclusions for full-scale web-core sandwich bridge decks.

1. Introduction

In the pursuit of more innovative and sustainable solutions for both bridge renovations and new construction projects, Fiber-reinforced polymer (FRP) or composite bridge decks have emerged as a compelling alternative to traditional materials due to fatigue and corrosion resistance, high strength-to-weight ratios, and minimal thermal expansion. Such attributes make composites an attractive option for replacing deteriorated timber, steel, or concrete decks while preserving the main structural elements of the bridge, like the primary girders and cross girders [1].

Bridge decks are critical components that endure constant wear, often worsened by increased traffic, leading to regular maintenance needs such as resurfacing, capacity upgrades to meet new codes, or corrosion prevention measures like painting steel girders. This ongoing maintenance not only disrupts traffic but also leads to economic and resource losses. With the rapid fabrication of composites and installation due to their lightweight nature, composite decks offer a potential solution to mitigate these disruptions and reduce long-term life-cycle costs [2,3].

The reduced weight of composite decks is particularly advantageous for both movable and fixed bridges, as it allows for the reuse of the existing structural foundations and mechanisms without significant modifications [4]. The early applications of composites in bridges focused on repairing, retrofitting, and strengthening existing structures [2,5]. However, the 1990s saw a shift towards using composites in bridge decks [6], with the 2000s marking the introduction of composites in new pedestrian and cyclist bridges [7]. Pultruded glass FRP (GFRP) decks have since gained interest due to their ability to be rapidly produced in complex shapes and installed in difficult-to-access locations.

Researchers [8,9] have explored various pultruded shapes and bonded profiles to meet the design requirements for bridge decks. However, challenges such as local buckling and delamination between webs and flanges have emerged, leading to challenges in deck designs [10–12]. This prompted the development of sandwich panels, which consist of a core material sandwiched between two facings. The stiff facings bear the flexural loads, while the low-density core material takes on shear loads, ensuring composite action between the top and bottom facings [2]. Materials like foams, honeycombs, balsa wood, and

* Corresponding author.
E-mail address: m.pavlovic@tudelft.nl (M. Pavlovic).

https://doi.org/10.1016/j.engstruct.2025.121117
Received 31 March 2025; Received in revised form 9 July 2025; Accepted 4 August 2025
Available online 20 August 2025

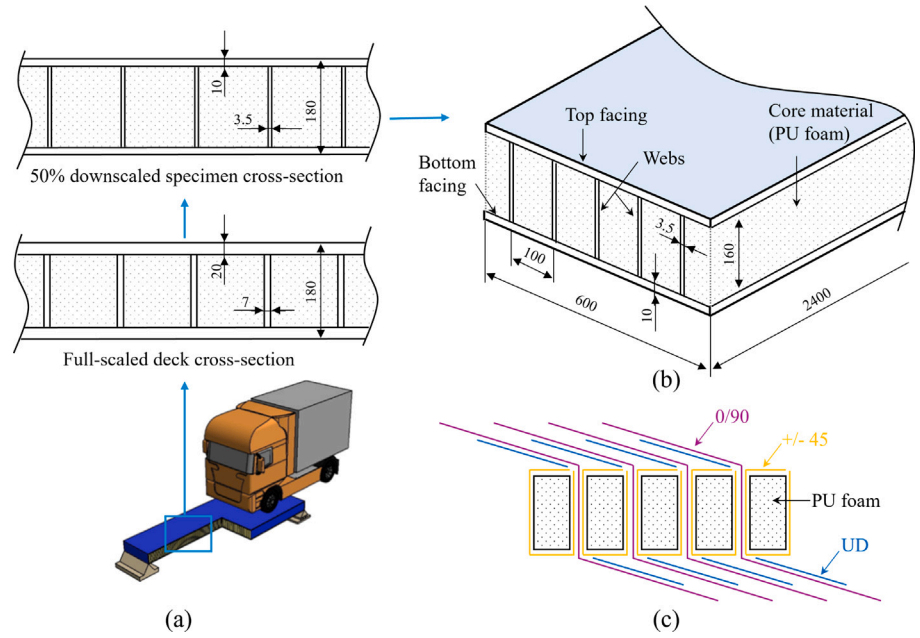

Fig. 1. Bridge deck (a) downscaling cross-section, (b) tested panel parameters, and (c) Z-shape layup by FiberCore. Dimensions are presented in mm.

cork are commonly used for the core [13]. GFRP webs oriented at ±45° have been designed to maximize shear properties.

Despite the promise of sandwich panels, limitations remain, particularly regarding load capacity, the quality control of production, and inconsistencies in fiber volume fractions in the webs [10]. With improved quality control, sandwich decks have met structural requirements for foot and cyclist bridges [7]. However, their application in road bridges presents new challenges, especially concerning fatigue performance under heavy traffic loads [14]. The lack of long-term data on the behavior of composites [15] in such settings has raised concerns about fatigue and displacement, drawing parallels to the fatigue issues previously experienced with steel bridges.

Unlike metals, which typically exhibit single-mode damage propagation, composites experience multiple fatigue mechanisms that accumulate over time, leading to failure. The viscoelastic nature of the polymer matrix further complicates predictions, as it is sensitive to temperature fluctuations and prone to creep effects [16]. Studies have shown anisotropic behavior in web-core sandwich panels used for bridge decks, with linear behavior in webs oriented longitudinally [17] and non-linear behavior with the webs in the transverse direction [18], primarily due to shear deformation.

As the European Committee for Standardization (CEN) works towards establishing design specifications for composite structures through Eurocodes, new qualification and proof testing requirements are being developed for products like web-core sandwich deck panels. However, current design recommendations offer limited guidance for early-stage composite designs, particularly regarding fatigue failure modes and stress concentrations at component connections. Testing remains essential but costly, highlighting the need for improved predictive models to evaluate fatigue performance during the design phase. Further research into the fatigue behavior of composite deck panels, particularly for main road applications, is crucial to enhancing the competitiveness and viability of these materials. Understanding the behavior of sandwich panels under fatigue loading is essential for improving their global fatigue performance and, by extension, the safety and longevity of composite bridge decks.

The presented study investigates the performance of bridge deck panels, comparing experimental results to European and Dutch design recommendations, particularly the upcoming Eurocode for composite structures (TS19101) [19] and the design guideline for composites (CUR96) [20]. The study explores the impact of imperfections on fatigue performance, supported by numerical analysis using Finite Element Modeling (FEM) that incorporates these factors to explore the interplay of failure mechanisms. Coupons are extracted from sandwich panels produced to identify whether imperfections are the primary driver behind the early failure of bridge decks subjected to cyclic loading conditions. A comprehensive experimental and numerical study of the static and fatigue resistance of the sandwich structure is conducted to contribute to the new developments in the designs, analysis, and production of composite bridge decks.

2. Materials and methods

Fig. 1 shows the cross-section of the tested sandwich panel. The web-core panels are in fact in orthotropic decks that are made of composites and not of steel. As such, structurally optimal is to provide them with boundary and support conditions by the bridge superstructure that favor load transfer in one direction, either in the longitudinal direction for simple bridges, or transverse in more complex bridge layouts. In this configuration, the bending and shear loads are primarily unidirectional, and thus the dominant stress components are captured effectively with a one-way bending setup. The developed experimental set-up is to replicate realistic service conditions observed in the field, where most critical failure modes (e.g., shear cracking in webs, facing wrinkling, local buckling) emerge primarily under longitudinal loading. The presented in this study specimen allows reproducible evaluation of static and fatigue resistance while ensuring consistency with both industry practice and relevant design guidelines (e.g., CUR96, TS19101).

2.1. Specimen description

The design of the sandwich panel in Fig. 1(a), the facing and web thicknesses, as well as the laminate architecture, was primarily guided by practical manufacturing processes and representative scaling of real bridge decks, rather than an explicit optimization-based structural design process. The facing and web thickness was intentionally reduced by approximately 50% compared to full-scale bridge decks to facilitate laboratory testing while still ensuring the capture of key failure modes (e.g., wrinkling, delamination, buckling). This downscaling approach enabled testing within the available loading capacity (up to 1000 kN)

Table 1
UD ply material properties.

Material	Longitudinal modulus, E_1 (GPa)	Transverse modulus, E_2 (GPa)	Shear modulus, G_{12} (GPa)	Poissons ratio, ν_{12} (–)	Density, ρ (kg/m^3)
Facings $V_f = 54\%$	42	14.5	4,2	0.27	1962
Webs $V_f = 27\%$	22	8	3,5	0.27	1576

Table 2
UD ply strength parameters.

Material	Tensile strength, (MPa)		Compressive strength, (MPa)		Shear strength, (MPa)	
	σ_{T1}	σ_{T2}	σ_{C1}	σ_{C2}	τ_{12}	τ_{13}
Facings $V_f = 54\%$	855	59	395	138	39	51
Webs $V_f = 27\%$	327	24	410	130	32	33

and specimen size limits at the Stevin II Laboratory in TU Delft. The web and facing thickness and lay-up were derived from standard manufacturing practice by FiberCore Europe and reflect typical geometry used in full-scale vacuum-assisted resin infused composite decks. The downscaled bridge deck segments, shown in Fig. 1(b), consist of web-core panels, which incorporate polyurethane (PU) foam blocks. The production of the panels by FiberCore Europe incorporated three types of fabrics: the PU foam blocks were wrapped with [+/−45] E-glass fabrics, and three layers of E-glass unidirectional (UD) fabrics along the length direction are added with a two PU block overlap at the top and bottom of each block. The Z-shape layup in Fig. 1(c) further involves the placement of two layers of E-glass [0/90] fabrics with a 2.5 PU block overlap. The laminated top and bottom facings and the webs of the deck have the lay-ups of $[((0/90)_2/0_3)_4/0/90/\pm 45]$ and $[\pm 45_2/(0/90)_2/\pm 45_2]$, respectively. These configurations ensure a balanced distribution of stiffness and strength in both longitudinal and transverse directions while maintaining manufacturing feasibility. The overall aim was to reproduce a representative structural response while embedding realistic imperfections and manufacturing features to assess the sensitivity of the system to fatigue and local failures, which are relevant for full-scale application scenarios.

Tables 1 and 2 provide the isotropic elastic material properties and strength parameters of the UD plies that compose the facings with fiber volume fraction of $V_f = 54\%$ and the webs with $V_f = 27\%$. The lower fiber volume fraction in the webs compared to the facings is primarily due to manufacturing constraints. The webs are fabricated by wrapping [+/−45] E-glass fabrics around PU foam cores, a process that inherently leads to reduced fiber compaction due to the complex geometry and the need to accommodate the foam interface. Subscripts '1', '2', and '12' in the Tables indicate the longitudinal, transverse, and shear properties, respectively. These properties are obtained from standard material tests conducted by the panel producer.

Once the reinforcement layers are properly positioned, the polyurethane resin is infused through two runners located 317.5 mm from the edge of the deck. The web-core panels are connected only by polyurethane resin during the infusion which bond the E-glass fiber fabrics (forming the webs and facings) to the PU foam core blocks. The bonding ensures integrity of the sandwich structure and composite action between the components. The polyurethane resin system used is a thermosetting polymer, which offers good mechanical performance under ambient conditions but is temperature sensitive. Elevated temperatures can lead to a reduction in modulus and strength, especially near or above the resin's glass transition temperature (Tg) in a range of 10%–30% according to the current design recommendations. However, in this study, the tests were conducted under standard laboratory conditions, well below the Tg of the resin system. Therefore, temperature-induced effects on the load-bearing capacity were not significant and can be safely neglected for the current scope.

Table 3
Material properties of steel and cork.

Property	Steel	Cork
Young's modulus, E (MPa)	210 000	30.8
Yield stress, f_x (GPa)	355	–
Poisson's ratio, ν_{12} (–)	0.3	0
Density, ρ (kg/m^3)	7800	2200

2.2. Test set-up

The tests are conducted at the Stevin Laboratory II at Technical University Delft, as depicted in Fig. 2. The test setup includes a specially designed loading steel frame to accommodate the specimen. All specimens undergo loading in a three-point bending configuration, with a span of 2 m with the webs in the longitudinal direction. The jack employed in the static experiments has a maximum stroke capacity of 100 mm and a maximum load capacity of 1000 kN; for the fatigue tests, the jack with a load capacity of 400 kN is used. To allow for minor lateral displacement and prevent torsion within the web-core sandwich panels, the panel is supported by two rollers. Steel 30 mm plates are positioned between the rollers and the composite panel to avoid force concentrations around the supports. The steel loading plate dimensions of 600 mm × 320 mm is used to apply the load. The dimensions of the plate were chosen based on a combination of experimental practicality and realistic simulation of tire contact area in accordance with Eurocode EN1991-2 [21] provisions for fatigue and local effects (FLM4). The width of 600 mm corresponds to the full width of the downscaled specimen to ensure a uniform load transfer across the cross section during testing and to avoid stress concentrations at the specimen edges. This approach allows for controlled and repeatable conditions in evaluating global panel behavior. The longitudinal length of 320 mm approximates the footprint of a typical truck tire under service conditions, which usually ranges from 250 mm to 350 mm according to FLM4 in the longitudinal direction depending on inflation and axle load. This size was selected to reasonably simulate the tire contact patch while also aligning with the stiffness and wrinkling sensitivity of the composite facings. To mitigate the wrinkling behavior, a cork interlayer was used between the steel plate and the composite panel to better distribute stresses and minimize artificial stress concentrations, as outlined in [22]. This configuration provides a balance between realistic loading and consistent testing conditions across specimens. The properties of the steel and the cork [23] are shown in Table 3. The tests are performed load-controlled, and the loads are measured until the panel completely fails. Two static tests are performed with a monotonic loading of 2.5 mm/min to failure. The peak loads of the tests provided an estimate of the ultimate static capacity, F_{ult}, of the panels. The fatigue tests are performed at the load ratio of R = 0.1 at a rate of 1 Hz. The tested fatigue loads are chosen between 40% and 20% of F_{ult}.

To measure the precise vertical deformation of the deck, four vertical linear potentiometers (LPs) are employed. These vertical LPs (named LP-V) are placed at three distinct locations at the panel depending on the loading protocol: at the midpoint (LP2-V and LP3-V), at one-quarter of the total length (LP4-V and LP5-V) and in the proximity of the supports (LP1-V and LP6-V), as shown in Fig. 3. During the static tests, vertical LP2-V - LP5-V are utilized. During the fatigue tests, four vertical LP1-V - LP3-V and LP6-V, and two longitudinal LPs-L, shown in Fig. 4, which are added on the bottom facing in the middle of the span are utilized.

3. Experimental results and discussion

3.1. Static test

Two static three-point bending tests to identify the F_{ult} are performed with the set-up in Fig. 2. The load–deflection curve in Fig. 5

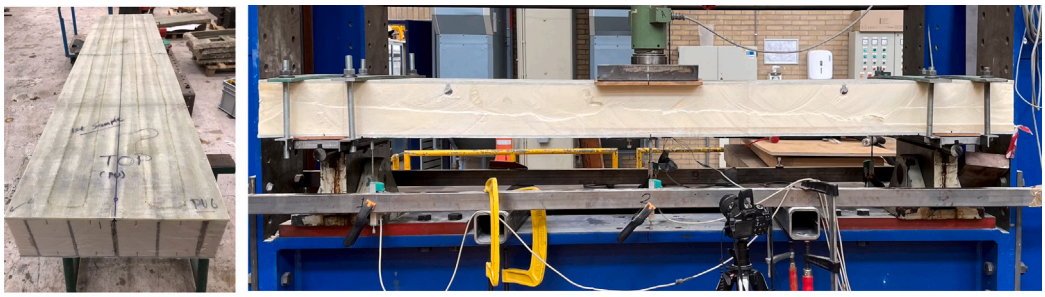

Fig. 2. (a) Web-core panel and (b) Experiments set-up.

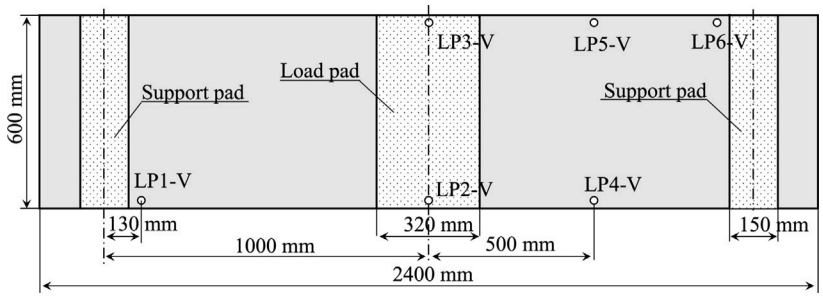

Fig. 3. Vertical LPs (LP-V) layout (sketch). Loads and supports.

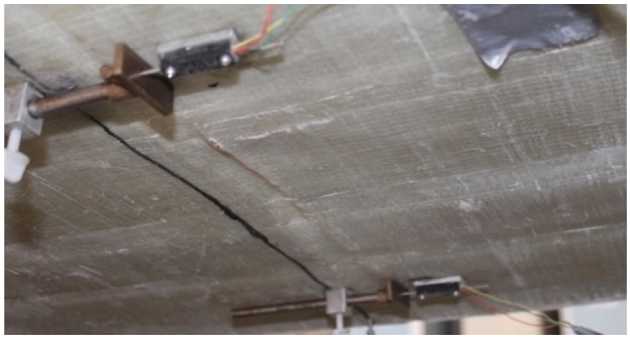

Fig. 4. Longitudinal LPs (LP-L).

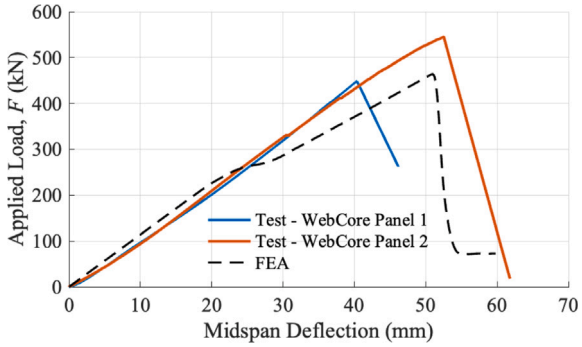

Fig. 5. Force–Displacement comparison between tests and FEA.

illustrates the behavior of the panels. The deflection of both panels show nearly linear characteristics, where the average displacement of LP2-V and LP3-V in the middle of the panel is considered for analysis. Panel 1 is failing under a load of $F_{ult}^{panel1} = 441$ kN and a displacement of 38 mm, while Panel 2 fails under a load of $F_{ult}^{panel2} = 545$ kN and a displacement of 53 mm. The presented Finite Element Analysis (FEA) results in Fig. 5 are discussed in Section 5. The deflection shows nearly linear characteristics,

After the visual inspection of the specimens described in [24], the failure mechanisms of web buckling, top layer buckling, and shear failure at the supports are found. The inspection of Deck 1, shown in Fig. 6(a) indicated the crushing of the webs at the runner, which is the suspected point of initiation of the failure mechanism for this specimen. The inspection of Deck 2 indicated the failure of the specimen due to the top-facing buckling and delamination, as shown in Fig. 6(b). The occurrence of a small nonlinear behavior prior to failure further supports the buckling failure mechanism. The absence of initial imperfections likely contributed to the higher ultimate load observed in this test of Panel 2.

3.2. Fatigue test

Four web-core sandwich panels are subjected to constant amplitude cycling loading of between 100 kN (20% of $F_{ult} = (F_{ult}^{panel1} + F_{ult}^{panel2})/2 =$ 493 kN) and 200 kN (40% of F_{ult}), as shown in Table 4. The tests resulted in Panel 3 failure after 37,949 cycles and Panel 4 – after 40,458 cycles under the tested load of $F_{max} = 200$ kN. Panel 5 is tested twice. Firstly, Panel 5 (referred to as Panel 5–1) is subjected to the $F_{max} =$ 100 kN, and the test is stopped after the life of 2.14 million cycles is reached without any visible crack, laminate discoloration or stiffness degradation. The load level of 100 kN led to no damage. Later, the same Panel 5 (referred to as Panel 5–2) is tested under the increased load of $F_{max} = 150$ kN until the failure. The fatigue life of Panel 5–2 is only 83,970 cycles less compared to Panel 6, which is tested under the same load and thus showed a similar fatigue life. Force-Life (F-N) curves and representative stresses at the bottom facing of the panel are presented in Fig. 7.

Based on the test data, F-N curve is constructed in accordance with the ASTM E739-10 standard [25]. The data for Panel 5–1 runout is excluded from the F-N curve. The derived slope of the curve indicated as $k = -7.72$, aligns closely with the CUR96 guideline [20], which

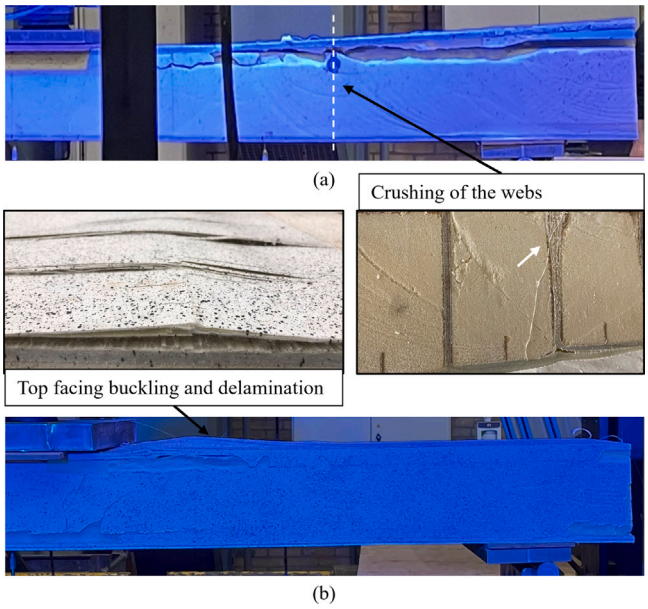

Fig. 6. Failure mechanisms in (a) Panel 1 and (b) Panel 2.

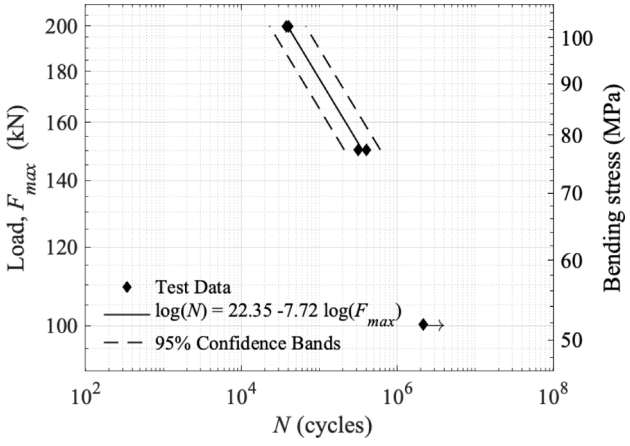

Fig. 7. F-N and S-N curves for tested web-core panel specimens.

Table 4
Fatigue life by experiments.

Panel	Applied load, F_{max} (kN)	Fatigue life, (cycles)	Initial imperfection
3	200	37,949	(at the mid span,
4	200	40,458	a local dimple
5–1	100	$2.14 \cdot 10^6$	of 1 mm depth
5–2	150	$3.72 \cdot 10^5$	across the width
6	150	$3.80 \cdot 10^5$	of all panels)

suggests a regression parameter of $k = -7$ for panels composed of laminate from glass fibers and polyester resin.

The captured failure in the panels in Fig. 8 is indicated by the rapid increase of global displacement measured by the LPs-V, shown in Fig. 9 and local displacement of the bottom facing measured by LPs-L, shown in Fig. 10. In all the tests, the panels started to crack on one edge of the specimen and propagated across the panel width till failure. For example, during the test of Panel 6, the crack development is noticed at the location of LP2-V just after $3 \cdot 10^5$ cycles, with the crack propagation through the width of the panel and reaching the other edge at around $3.8 \cdot 10^5$ cycles.

The degradation of the structural properties during the fatigue loading is periodically monitored. The relative stiffness of the web-core sandwich panels is assessed at cycles N_i, and Fig. 11 shows the evolution of the normalized stiffness K_i/K_0, where K_0 is the stiffness obtained in the initial cycle. The stiffness degradation of composite panels is a critical aspect that must be considered when evaluating the performance and longevity of web-core composite structures. Over time, composite materials may experience a reduction in stiffness under the accumulated fatigue damage, leading to reduced structural performance.

This degradation directly impacts the relative stiffness between the core and facings, potentially altering the load distribution and increasing the risk of localized failures. Fig. 11(a) includes the global stiffness degradation of the panel, where LPs-V are considered. It can be seen that global stiffness reduction is around 8%, followed by a maximum stiffness drop and failure. Evaluating the local (considering LPs-L) stiffness degradation in Fig. 11(b) of the bottom facing in the region of the crack development indicated that the final failure occurs after the local stiffness reduction of around 15%. The data for Panel 5–1 is missing due to the LP malfunctioning during the test, as can be seen in Fig. 10(e).

4. Finite element model description

FEA is conducted in ABAQUS/Standard on the web-core sandwich panels to determine the maximum failure loads and corresponding displacements. Given the large scale of the bridge decks and the intricate structural behavior of the panels, it is crucial to analyze complex structures using analytical methods and establish predictive FEMs. The panel's webs and facings are simulated with 2-D orthotropic, linear elastic, non-layered S4R shell elements with a 30 mm mesh. The composite laminate of these parts consists of layered plies with defined orientation. The panel's facings comprise 32 layers, with ±45° plies considered as a single layer split into +45° and −45° for detailed modeling, each half maintaining the collective thickness of the other layers. The webs follow a similar structure with 8 total layers. The facings and webs are oriented such that direction 1 aligns with the UD fibers, direction 2 is perpendicular, and direction 3 is through the thickness, as per predefined local orientations. Ply properties are shown in Table 1. Damage evolution adopts Hashin's criteria with longitudinal fracture energy at 100 N/mm and transverse fracture energy at 0.969 N/mm [26]. The following model is applied to the progressive damage analysis on the ply level.

In the current FEA, the PU foam blocks are not explicitly modeled. This simplification is made to reduce computational complexity and focus the analysis on the ply-level behavior of the GFRP facings and webs, particularly in relation to imperfections and fatigue performance. With respect to buckling behavior, the foam core primarily contributes to the post-buckling enhancement of the performance. To capture this behavior, non-linear FE buckling analysis with integrated imperfections would be required. Therefore, this is not the scope of this study.

The panel is modeled as shown in Fig. 12(a), with roller supports and using two cork pads. The cork pads are meshed with solid C3D8R elements, using a 20 mm mesh size and two elements through the thickness. The cork pads are fixed in the y-direction and constrained rotationally in the z-direction. Constraints are applied through reference points, which are connected to the bottom surface of the cork pads.

The steel plate for the wheel load is modeled using S4R shell elements with a 15 mm mesh size positioned at the panel's mid-span. A cork pad is modeled with solid C3D8R elements between the steel plate and the panel. These elements are assigned linear elastic properties according to Table 3. The load is applied to a 60 mm radius circular section of the plate, ensuring accurate load application as per the experimental setup, which is rigidly connected to a central reference point. The load is applied through a prescribed downward displacement of the central reference point. All other translations and rotations

Fig. 8. Failure mechanism due to fatigue.

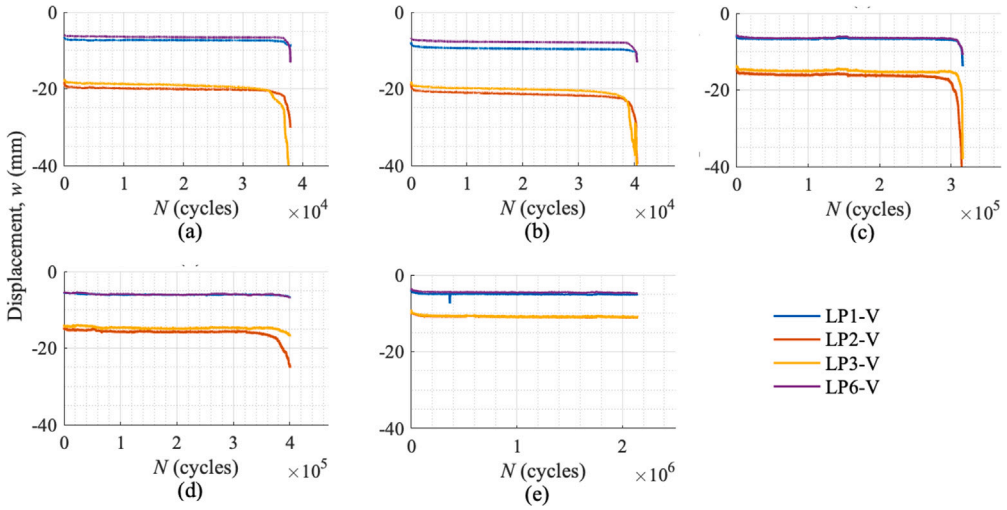

Fig. 9. Panel displacements from LPs-V for web-core sandwich (a) Panel 3, F_{max} = 200 kN, (b) Panel 4, F_{max} = 200 kN, (c) Panel 5–2, F_{max} = 150 kN, (d) Panel 6, F_{max} = 150 kN, (e) Panel 5–1, F_{max} = 100 kN.

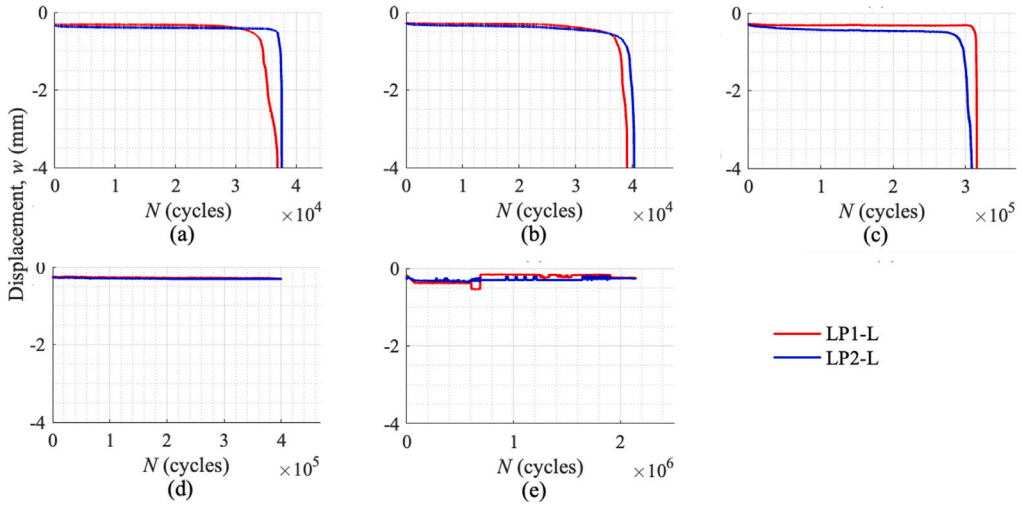

Fig. 10. Panel displacements from LPs-L for web-core sandwich (a) Panel 3, (b) Panel 4, (c) Panel 5–2, (d) Panel 6, (e) Panel 5–1.

restrained. Tie constraints connect the steel plate, cork pads, and panel surfaces. Within these constraints, the cork elements are designated as secondary components, maintaining a subordinate position in the master–slave hierarchy.

The evaluation of the tests in Section 3 and the visual inspection of the panels showed the imperfection on the bottom facing, as shown in Fig. 4, where during the dynamic loading, the crack initiation and propagation occurred, as shown in Fig. 8. To investigate the effect of this imperfection, two FE models are developed with different levels of damage and imperfection. The damage analysis is purely for constitutive modeling purposes and does not refer to any external damage exerted on the panel. Damage modeling is used to bridge the gap in assessing fatigue behavior between the ply and laminate level analyses.

The analysis will consider three types of models to evaluate the structural behavior of laminated composite panels under different conditions. Model 1 represents the full panel from Fig. 12(a) with original, undamaged ply properties (no discount), as shown in Table 1, serving as the baseline.

Model 2 is the full panel Model 1 with reduced ply properties (limited discount method, assuming complete damage in the off-axis direction). The CUR96 [20] recommendation defines S-N curves in the function of UD plies loaded in the direction of fibers and it is unspecified how to handle multidirectional laminates. To this end,

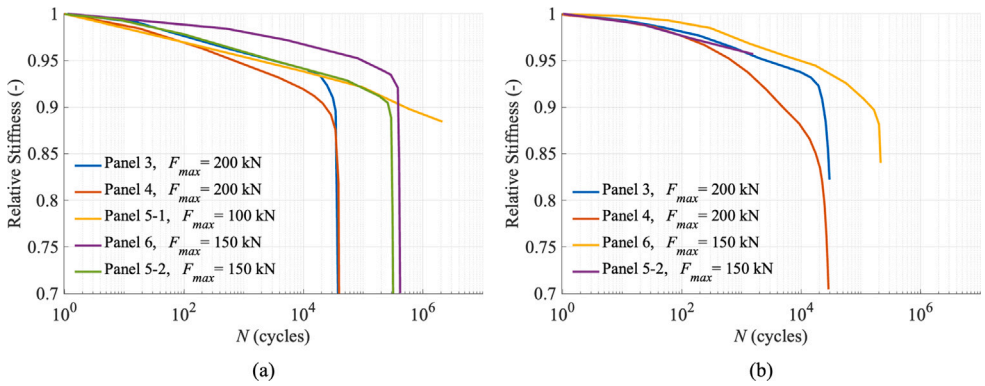

Fig. 11. Relative stiffness of the panels considering (a) global vertical displacement and (b) local (bottom facing) differential longitudinal displacement.

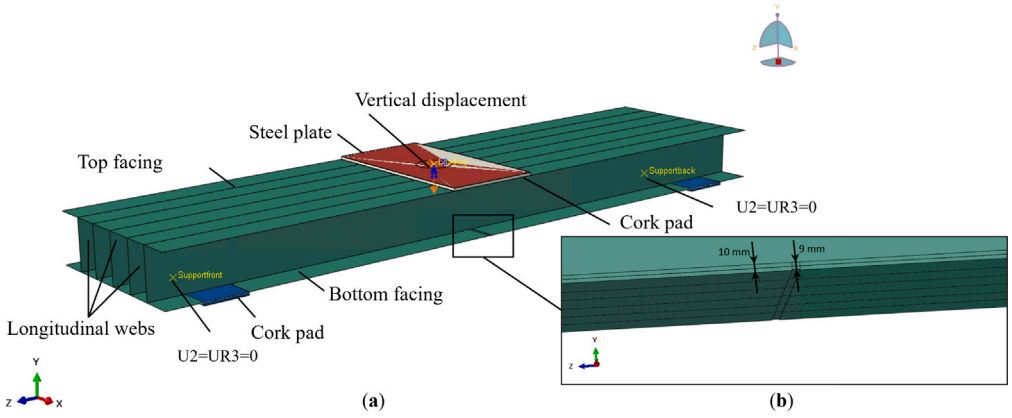

Fig. 12. FE model: (a) boundary conditions and (b) region of imperfection.

in the fashion of well-established procedures for progressive failure analyses, the stiffness of the plies in multi-directional laminates will be reduced in the off-axis direction. The assumption is that during the load cycles, the matrix-dominated stiffness in transverse tension and compression and in-plane shear of the UD-ply will be degraded significantly due to micro-cracks. The result is that the only load-carrying constituent in a multi-directional laminate subject to fatigue is the fibers. To replicate such behavior in the model, the transverse and shear stiffness of the plies (E22 and G12) are greatly reduced in this analysis. The stresses in plies are determined in the models with reduced ply properties. The transverse modulus and shear modulus of the facings are reduced by a factor of 1000, resulting in $E_2 = 14.5$ MPa and $G_{12} = 4.2$ MPa.

Model 3 is the full panel Model 1 with reduced ply properties and imperfection at the bottom facings, as shown in Fig. 12(b). After visually analyzing the imperfection running through the bottom facing of the panel, a 1 mm imperfection, such as local dimple across the width of the panel, is introduced in the analysis. This is implemented by localy reducing the bottom facing thickness in the model, altering the ply thicknesses and introducing eccentricity. The eccentricity can further increase stress in certain plies beyond the stress increase caused solely by the reduction in cross-sectional area. The material properties are changed with the longitudinal modulus increased by 10%, resulting in $E_{1,imp} = 46.67$ GPa. The reduced ply properties are in line with the CUR96 recommendations, where it is assumed that fibers in the transverse direction are completely degraded due to micro-cracks between the fibers in fatigue loading. This will result in all the strains being transferred by the fibers in the longitudinal direction (e.g., there will be no stiffness in the transverse and shear directions).

5. Resistance of the deck by FEA and CUR96

5.1. Static resistance by FEA

To validate the FE model the force–displacement is compared to the experiments. The predicted force–deflection behavior by FEA for a panel of 2.4 m (Model 1) is shown in Fig. 5. The reaction forces are picked at the reference point, and the deflections are picked from the middle of the bottom facing. According to the FEA, the final failure of the panel occurred at the applied load of 462 kN with the deflection of the bottom facing of 51 mm. To assess the structural integrity of the panel, the governing stresses in the facings and webs are analyzed. The maximum stresses S_{11}, S_{22}, and S_{12} in Figs. 13–15 are shown on ply level as maximum values that reside at each location from the entire laminate. The summary of the maximum stresses and the failure locations are shown in Tables 5–7, where the values in the brackets are the strength of the laminate from Table 1. The material is considered elastic until the failure criteria are reached. The stress failure considering S_{11} stresses occurs first in the webs, which have reached the longitudinal tensile strength of 327 MPa. The analysis of the S_{22} stresses indicated the highest stresses of 59 MPa at the bottom facing at the region of the supports. The following damage would not occur in the real set-up and is occurring in the FEA only due to the defined boundary conditions. Instead, the stresses of −126.9 MPa in the webs are very close to the transverse compressive strength of 130 MPa, with the failure occurring in the regions below the corners of the loading plate. According to the analysis of the S_{12} stresses, the highest maximum and minimum stresses are observed in the webs near the loading plate.

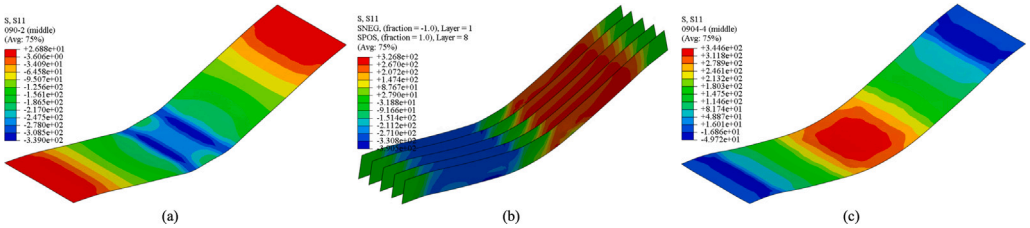

Fig. 13. S_{11} stresses in the plies at (a) top facing, (b) webs, (c) bottom facing.

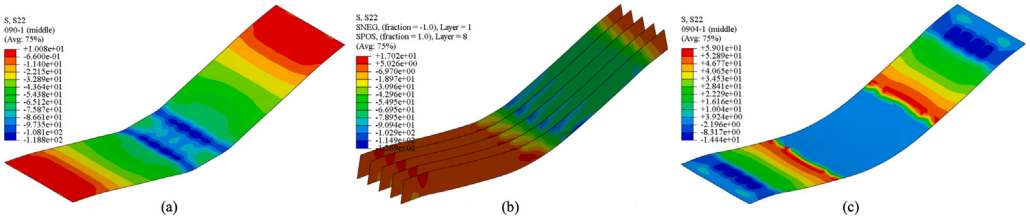

Fig. 14. S_{22} stresses in the plies at (a) top facing, (b) webs, (c) bottom facing.

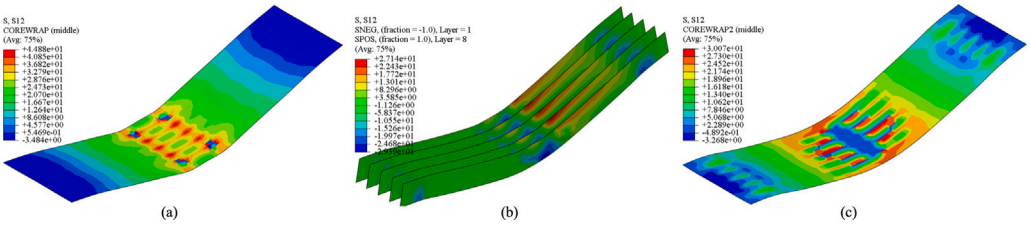

Fig. 15. S_{12} stresses in the plies at (a) top facing, (b) webs, (c) bottom facing.

Table 5
σ_{11} stresses by FEA.

	σ_{max} (MPa)	σ_{min} (MPa)	Failure at
Top facing	26.88 (855)	−339.0 (−395)	0° top ply
Webs	326.8 (327)	−390.5 (−410)	±45° ply
Bottom facing	344.6 (855)	−49.72 (−395)	0° bottom ply

Table 6
σ_{22} stresses by FEA.

	σ_{max} (MPa)	σ_{min} (MPa)	Failure at
Top facing	10.08 (59)	−118.8 (−138)	90° top ply
Webs	17.02 (24)	−126.9 (−130)	±45° ply
Bottom facing	59.01 (59)	−14.44 (−138)	90° bottom ply

Table 7
σ_{12} stresses by FEA.

	σ_{max} (MPa)	σ_{min} (MPa)	Failure at
Top facing	44.88 (398)	−3.48 (−398)	±45° ply
Webs	27.14 (32)	−29.39 (−32)	±45° ply
Bottom facing	30.07 (398)	−3.26 (−398)	±45° ply

5.2. Buckling resistance

The buckling resistance is predicted based on the new Eurocode Technical Specifications (TS) for composite structures [19]. Web-core sandwich panels consist of cells between the webs filled with PU foam, enhancing their structural integrity. The PU foam core provides a significant lateral restraint to the FRP webs, which has a direct stabilizing effect on their flexural (local buckling) behavior. Therefore, this constraining effect is not captured in the simplified analytical shear buckling formulas in TS, which assume unrestrained web edges. Both the experimental results and the FEA (which did not predict buckling) confirm that the foam significantly delays or suppresses local instability of the webs.

Table 8
Homogenized laminate properties.

Material	Long. modulus E_1 (GPa)	Trans. E_2 (GPa)	Shear G_{12} (GPa)	Poissons ratio ν_{12} (–)	Long. strength σ_{T1} (MPa)	Trans. σ_{T2} (MPa)	Shear τ_{12} (MPa)
Facings $V_f = 54\%$	33.41	22.76	4.5	0.18	401	273	72
Webs $V_f = 27\%$	12.83	12.83	5.06	0.27	154	154	80.9

The verification of global stability in web-core sandwich panels considers interactions between axial, shear, and transverse loads while incorporating boundary conditions, following an approach similar to that used for hollow sections. The panel's cross-section is analyzed as a hollow section to account for its structural response under loading. The dimensions of the hollow section are the following: the thickness and the width of the top and bottom facings are t_f = 10 mm and b_f = 100 mm, respectively; the thickness and the height of the webs are t_w = 3.5 mm and b_w = 170 mm, respectively. For the analysis, the homogenized properties of the laminate are used, shown in Table 8, obtained by Classical Laminate Theory. Those properties are based on the actual layups of the facings and webs. The homogenized values represent the effective in-plane properties of the multi-directional laminate, not the raw UD ply, as indicated in Table 1. The apparent reduction in stiffness or strength in Table 8 arises naturally due to the presence of off-axis plies (±45°, 90°), which reduce the effective stiffness in the loading direction when averaged across the laminate stack.

5.2.1. Local stability due to bending

According to TS, the design buckling resistance of the cross-section should be obtained taking into account the critical stresses for buckling

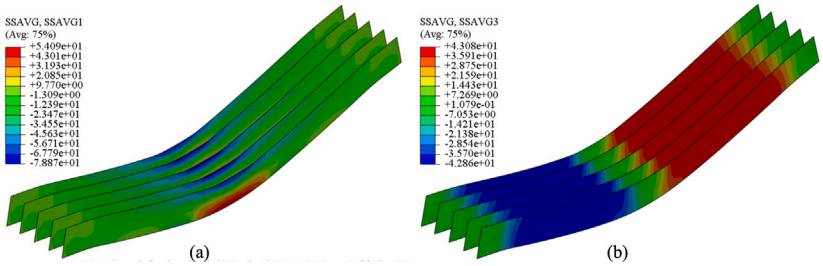

Fig. 16. Average (a) longitudinal and (b) shear stresses in the webs.

of the flange and the web. The interaction between the local buckling of the web and the flange is evaluated according to Kollar's approach. The critical buckling stresses of the flange and the web are 739.47 MPa and 122.28 MPa, respectively, which were determined in Eqs. (1) and (2), assuming simply supported boundary conditions between them.

$$(f_x)_f = \frac{\pi^2}{t_f \cdot (b_f - t_w)^2} \cdot [2\sqrt{(D_{11})_f (D_{22})_f} + 2\left((D_{12})_f + 2(D_{66})_f\right)] \quad (1)$$

$$(f_x)_w = \frac{\pi^2}{t_w \cdot b_w^2} \cdot \left[13.4\sqrt{(D_{11})_w \cdot (D_{22})_w} + 10.4\left((D_{12})_w + 2(D_{66})_w\right)\right] \quad (2)$$

where D_{11}, D_{22}, D_{12} and D_{66} are the stiffness matrices for flanges ('f') and webs ('w'). The critical stresses for the web are lower than the flange, meaning the web buckles first. The critical stresses of the web will be increased due to the interaction with the flange, but no closed-form solution is available for a plate with rotationally restrained edges subjected to linearly varying normal force. Therefore, as a conservative estimate, the web is considered as simply supported on longitudinal edges, not being rotationally restrained by the facings, and the critical buckling stress is considered as 122.28 MPa.

FEA indicated that the maximum longitudinal stress in the webs due to the global bending of the panel is 53.97 MPa (Fig. 16(a) at the load level of 462 kN). The longitudinal stresses of 53.97 MPa is lower compared to the evaluated critical stresses in the webs by TS. The failure in the structure occurs due to material failure and not due to local buckling.

5.2.2. Local stability due to shear

The analysis of the critical shear force of the cross-section is performed according to the TS, where both edges are clamped. Under the selected boundary conditions, the parameter $K > 1$ (Eq. (3)), where $N_{xy,cr} = 150.6$ MPa is evaluated according to Eq. (4). The shear buckling resistance of the web according to TS is $(f_{k,cr})_w = N_{xy,cr}/t_w = 43.03$ MPa. Therefore, FEA predicts shear buckling in the web at a stress level of 43.08 MPa, shown in Fig. 16(b), corresponding to an applied load of 237 kN. The experimental data and FEA indicate that panel failure is precipitated by loads exceeding 237 kN rather than by buckling of the web itself. Two critical considerations during the FEA are noted: (1) the foam core blocks are excluded from the analysis to simplify the model; (2) the buckling analysis methodology employed by the TS, relying only on the linear elastic buckling, is conservative (safe) when applied to slender structural elements.

$$K = \frac{2 \cdot (D_{66})_{wx} + (D_{12})_{wx}}{\sqrt{(D_{11})_{wx} \cdot (D_{22})_{wx}}} = 1.37 \quad (3)$$

$$N_{xy,cr} = \frac{4}{b_w^2} \cdot \left[\sqrt{(D_{22})_w \cdot \left((D_{12})_w + 2 \cdot (D_{66})_w\right)} \cdot \left(18.6 + \frac{3.56}{K^2}\right)\right] \quad (4)$$

Table 9
Fatigue life prediction by FEA.

Force F_{max}, (kN)	Model 1 (no discount)	Model 2 (limited discount)	Model 3 (discount+imperfection)
	Maximum stress, σ_{max} (MPa)		
150	106.9	163.7	244.8
200	137.2	205.8	294.8
	Fatigue life, 10^6 (cycles)		
150	34.48	1.75	0.10
200	6.02	0.35	0.03

5.3. Fatigue endurance

The analysis of the fatigue life of the panels is performed according to CUR96 [20], where the relation between maximum load and the number of cycles to failure is presented by the double logarithmic law shown in Eq. (5). This criterion is meant to be used on the ply level to analyze the fatigue of the laminate in a structure.

$$\log(N) = k \cdot \log\left(\frac{\gamma_{Mf} \cdot \gamma_M \cdot \sigma_{\max}}{\eta_c \cdot B}\right) \quad (5)$$

where N - is the number of cycles to failure; k – is the regression parameter, derived from the tests; B – is the characteristic strength of the laminate after one cycle, the characteristic static strength of the laminate can be assumed; $\sigma_{\max}$ – is the maximum stress acting during a cycle; γ_{Mf} – fatigue material factor = 1.0 if the variation of the measured stress for a specific number of cycles is no more than 10% to 20%; γ_M – conversion factor; η_c – partial material factor.

To perform the comparative study with experiments, the factors are selected as $\gamma_{Mf} = 1$, $\gamma_M = 1$ and $\eta_c = 1$, where the experiments are performed in the labs under the controlled loading and environmental conditions with no effect of moisture or temperature. The panel laminate is produced from glass fabrics and polyester resin, and the regression parameters for R = 0.1 are selected as $k = -7$ and $B = 1300 \cdot (0.54/0.55) = 1276$ according to the Tables 6–7 of [20].

Figs. 17 and 18 show the peak stresses at the center of the bottom facing for Model 1 (no discount), Model 2 (limited discount) and Model 3 (discount+imperfection), as discussed in Section 4. The stress at maximum experimental forces of $F_{max} = 150$ kN and $F_{max} = 200$ kN are interpolated and shown in Table 9. As shown in Fig. 19, Model 1 over-predicts the fatigue performance of the panels compared to the experimental data. Instead, using the Model 2, the stresses increased by a factor of 1.53 (163.7/106.9) compared to the Model 1. However, the number of cycles obtained with Model 2 are still over-predicted compared to the fatigue performance of the panels in the experiments. Utilizing Model 3 with the imperfection at the bottom facing shows a clear impact on the fatigue response of the panel. The stresses are increased by a factor of 2.29 (244.8/106.9) compared to Model 1 and by a factor of 1.5 compared to Model 2. The fatigue life is close to the experimental data shown in Fig. 19.

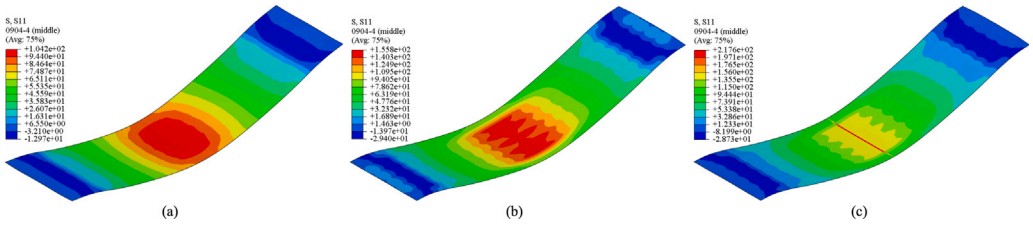

Fig. 17. Stresses at the bottom facing for (a) Model 1 at F = 145.5 kN, (b) Model 2 at F = 140.6 kN, and (c) Model 3 at F = 140.6 kN.

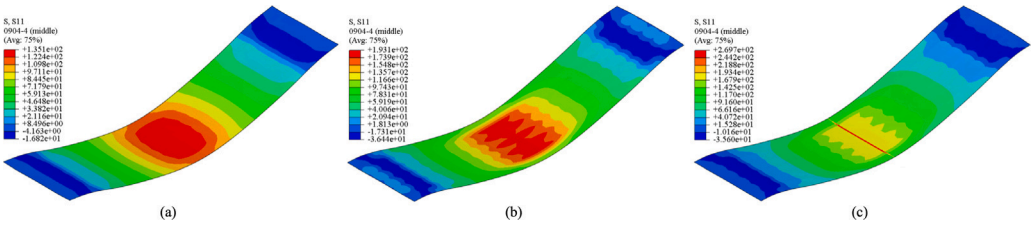

Fig. 18. Stresses at the bottom facing for (a) Model 1 at F = 196.5 kN, (b) Model 2 at F = 184.9 kN, and (c) Model 3 at F = 184.9 kN.

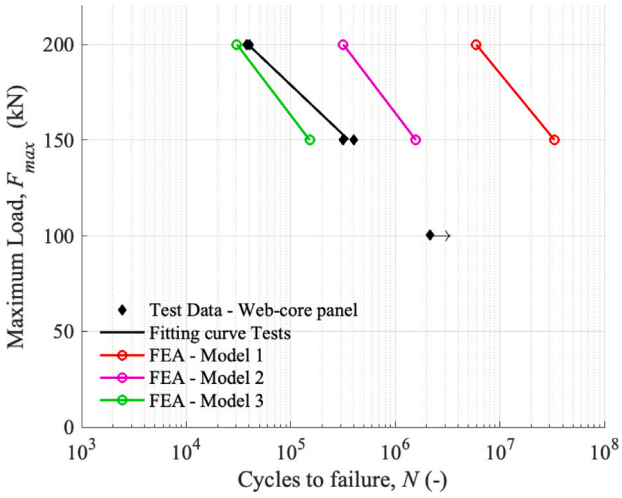

Fig. 19. F-N curves. Tests and FE predictions.

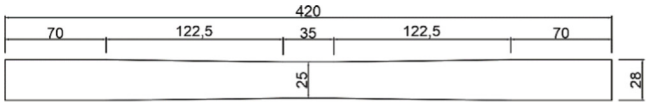

Fig. 20. Coupon specimens dimensions.

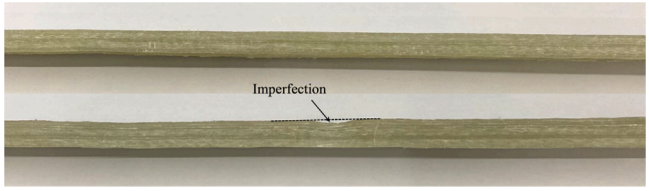

Fig. 21. Coupon specimens without and with imperfection.

6. Discussion

It is important to note that the tested panels are not full-scale bridge deck panels. The facing and web thickness were reduced by approximately 50% (downscaled) to ensure feasibility in laboratory testing. As a result, the influence of imperfections may be more pronounced due to the relatively thin facings. It is suspected that dimple imperfections have a reduced effect on thicker laminates used in full-scale bridge deck panels.

During the inspection of the manufactured panels, localized thinning was detected only in areas where the vacuum infusion hose ran beneath the panel. This imperfection was observed exclusively in the downscaled web-core sandwich panels and not in full-scale bridge decks. Consequently, FEA results, as shown in Fig. 19, clearly demonstrate the impact of this imperfection on the fatigue life of the panels.

The induced imperfection, appearing as a local dimple of approximately 1 mm across the width of the panel, led to a localized reduction in laminate thickness. In the FEM, the stiffness of the plies in the imperfection region was increased to account for the higher fiber volume fraction, under the assumption that the same amount of fibers is present despite the reduced thickness. With the adopted modeling approach in Model 3, the FE results closely align with experimental findings for web-core sandwich panels.

Since failure occurred at the bottom facings in the imperfection location, further investigation was conducted by extracting coupons from both the top and bottom facings of the manufactured panels. These coupons were precisely cut using a water jet technique from square panel facings, ensuring that the specimen dimensions comply with the ISO 527–4 standard [27], as shown in Fig. 20.

Additionally, Fig. 21 illustrates coupons extracted from the panels, both with and without imperfections.

The tensile–tensile fatigue coupon tests are performed under the R = 0.1 on a universal testing machine with a 250 kN load cell at different load levels and frequencies in accordance with ISO 13003 [28]. The load levels and loading frequencies are from 22% to 52% of the ultimate static capacity and 2 to 8 Hz. All tests are carried out in the load control mode with a sinusoidal waveform of constant amplitude. An extensometer with a gauge length of 50 mm is used during the tests. More details on the coupon material tests are provided in the accompanied paper of the authors (submission pending).

The experimental results on the coupons are shown in Fig. 22. The test data for coupons without imperfections showed a less steep S-N curve. The data points have a relatively longer fatigue life across a range of stress levels compared to coupons with imperfections. The coupons with imperfections showed a notably steeper slope in their S-N curve. The reduction in fatigue life is especially evident in the lowest tested load, where the fatigue life is reduced by a factor of 11 for

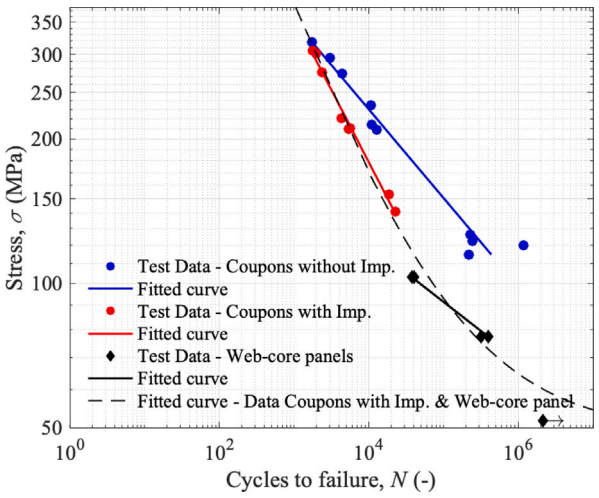

Fig. 22. S-N curves. Experimental data on coupons and web-core sandwich panels.

coupons with imperfections compared to those without. The web-core sandwich panels showed similar fatigue behavior to the coupons with imperfections, which is indicated by the fitted curve closely following the trend of the data points for coupons with imperfections. This suggests that imperfections, such as the dimples at the bottom facing of the panels, are significantly contributing to the reduction in fatigue life.

7. Conclusion

Static and fatigue performance of the composite web-core sandwich panels is investigated through experiments on downscaled panel specimens, coupon test results and FE modeling of the downscaled panel. The downscaling is done for the purpose of testing feasibility and obtaining the failure modes such that those can be further analyzed and understood. The real bridge deck would resist much larger forces.

The following conclusions can be drawn:

- High static capacity: The panels exhibited ultimate loads exceeding 493 kN, which is approximately 10 times higher than the fatigue design wheel load (FLM4: 0.5*90 kN) and 4 times higher than the LM2 local wheel load (0.5*200 kN), confirming strong potential for real-world applications. Static tests revealed competing failure mechanisms (e.g., web crushing, top-facing buckling, shear near supports).
- No shear buckling despite conservative predictions: Although Eurocode (TS19101) predicted web shear buckling at lower loads, this failure mode was not observed in either the experiments or FEA. This discrepancy suggests that the buckling analysis methods prescribed by the TS19101 can be conservative (safe) by neglecting the presence of the foam, especially for slender structural elements.
- Effect of imperfections on fatigue life: Local dimples on the bottom facing significantly reduced fatigue life. FEA predicted a 1.4 × increase in local stress and up to 10 × reduction in fatigue life, consistent with experimental observations.
- Validation of ply-level fatigue modeling: A good match was found between experimental fatigue data and FEA using ply-level analysis with off-axis stiffness discounting. The experimental F–N slope of 7.72 aligned well with the CUR96 guideline slope of 7. In addition, it is found that the ply-level CUR96 S-N curves can be applied to analyze fatigue of a multi-directional laminate using the ply-level analysis with an off-axis stiffness discount method examined in this work.
- Consistent trends in coupon tests: Imperfect coupons exhibited a similar degradation trend to the full panels, reinforcing that imperfections are critical in determining fatigue performance.
- Damage progression observed: Fatigue failure initiated at panel edges and propagated gradually, supporting the potential for damage-tolerant design approaches in sandwich panel systems.

Furthermore, further research is necessary on the web-core sandwich panels in order to confirm those findings.

CRediT authorship contribution statement

Olena Karpenko: Writing – review & editing, Writing – original draft, Visualization, Validation, Methodology, Investigation, Data curation. **Marko Pavlovic:** Writing – review & editing, Supervision, Resources, Project administration, Methodology, Formal analysis.

Declaration of competing interest

The authors declare that they have no known competing financial interests or personal relationships that could have appeared to influence the work reported in this paper.

Acknowledgments

The authors would like to express their gratitude to Rijkswaterstaat, the Directorate-General of the Ministry of Infrastructure and Water Management of the Netherlands for the financial support, and FiberCore Europe for the production of the panels.

Data availability

Data will be made available on request.

References

[1] Sonnenschein R, Gajdosova K, Holly I. FRP composites and their using in the construction of bridges. Procedia Eng 2016;161:477–82.
[2] Bakis CE, Bank LC, Brown V, Cosenza E, Davalos J, Lesko J, Machida A, Rizkalla S, Triantafillou T. Fiber-reinforced polymer composites for construction—State-of-the-art review. J Compos Constr 2002;6(2):73–87.
[3] Mara V, Haghani R, Harryson P. Bridge decks of fibre reinforced polymer (FRP): A sustainable solution. Constr Build Mater 2014;50:190–9.
[4] Burgoyne CJ. Advanced composites in civil engineering in Europe. Struct Eng Int 1999;9(4):267–73.
[5] Kim YJ. Advanced composites in bridge construction and repair, vol. 50, Elsevier; 2014.
[6] Hollaway L. The evolution of and the way forward for advanced polymer composites in the civil infrastructure. Constr Build Mater 2003;17(6–7):365–78.
[7] Qureshi J. A review of fibre reinforced polymer bridges. Fibers 2023;11(5):40.
[8] Saleem MA, Zafar MN, Saleem MM, Xia J. Recent developments in the prefabricated bridge deck systems. Case Stud Constr Mater 2021;15:e00750.
[9] Vedernikov A, Safonov A, Tucci F, Carlone P, Akhatov I. Pultruded materials and structures: A review. J Compos Mater 2020;54(26):4081–117.
[10] Mara V, Haghani R. Review of FRP decks: Structural and in-service performance. In: Proceedings of the institution of civil engineers-bridge engineering. vol. 168, Thomas Telford Ltd; 2015, p. 308–29.
[11] Xin H, Mosallam A, Liu Y, Xiao Y, He J, Wang C, Jiang Z. Experimental and numerical investigation on in-plane compression and shear performance of a pultruded GFRP composite bridge deck. Compos Struct 2017;180:914–32.
[12] Sharaf T, Fam A. Analysis of large scale cladding sandwich panels composed of GFRP skins and ribs and polyurethane foam core. Thin-Walled Struct 2013;71:91–101.
[13] Mottram J, Henderson J. Fibre-reinforced polymer bridges—guidance for designers. London, UK: CIRIA; 2018.
[14] Alampalli S, Kunin J. Load testing of an FRP bridge deck on a truss bridge. Appl Compos Mater 2003;10:85–102.
[15] Jollivet T, Peyrac C, Lefebvre F. Damage of composite materials. Procedia Eng 2013;66:746–58.
[16] Garrido M, Correia JR, Keller T, Cabral-Fonseca S. Creep of sandwich panels with longitudinal reinforcement ribs for civil engineering applications: experiments and composite creep modeling. J Compos Constr 2017;21(1):04016074.

[17] Kulpa M, Siwowski T. Stiffness and strength evaluation of a novel FRP sandwich panel for bridge redecking. Compos Part B: Eng 2019;167:207–20.
[18] Zi G, Kim BM, Hwang YK, Lee YH. The static behavior of a modular foam-filled GFRP bridge deck with a strong web-flange joint. Compos Struct 2008;85(2):155–63.
[19] CEN/TS19101:2022. Design of fibre-polymer composite structures. Technical xommittee CEN/TC 250 "Structural Eurocodes", Brussels, Belgium: European Committee for Standardization; 2022.
[20] CROW-CUR Recommendation 96:2019. Fibre-reinforced polymers in buildings and civil engineering structures. 2019, CROW-CUR.
[21] European Committee for Standardization. Eurocode 1 - actions on structures - part 2: Traffic loads on bridges and other civil engineering works. 2021, Standard No. EN 1991-2.
[22] Sebastian W, Ralph M, Poulton M, Goacher J. Lab and field studies into effectiveness of flat steel plate–rubber pad systems as tyre substitutes for local loading of cellular GFRP bridge decking. Compos Part B: Eng 2017;125:100–22.
[23] Anjos O, Pereira H, Rosa ME. Tensile properties of cork in axial stress and influence of porosity, density, quality and radial position in the plank. Eur J Wood Wood Prod 2010;69(1):85–91.
[24] Karpenko O, Peeters T, Christoforidou A, Pavlović M. Fatigue of web-core composite bridge decks - an experimental and numerical study. In: CICE 2023 single volume proceedings. 11th international conference on fiber-reinforced polymer (FRP) composites in civil engineering (cICE 2023), Brazil. Zenodo; 2023.
[25] ASTM E739-10. Standard practice for statistical analysis of linear or linearized stress-life (S-N) and strain-life (ϵ-N) fatigue data. ASTM International; 2010.
[26] Xin H, Mosallam A, Liu Y, Wang C, Zhang Y. Analytical and experimental evaluation of flexural behavior of FRP pultruded composite profiles for bridge deck structural design. Constr Build Mater 2017;150:123–49.
[27] ISO 527-4:2023. Part 4: Test conditions for isotropic and orthotropic fibre-reinforced plastic composites. ISO International; 2023.
[28] ISO 13003. Fibre-reinforced plastics - Determination of fatigue properties under cyclic loading conditions. ISO International; 2003.